Discover Nano

Discover

Research

Room-temperature ammonia gas sensing via Au nanoparticle-decorated TiO_2 nanosheets

Jeong Yun Hwang[1] · Yerin Lee[1] · Gyu Ho Lee[1] · Seung Yong Lee[1,2] · Hyun-Sik Kim[3] · Sang-il Kim[3] · Hee Jung Park[4] · Sun-Jae Kim[5] · Beom Zoo Lee[6] · Myung Sik Choi[7] · Changhyun Jin[1] · Kyu Hyoung Lee[1]

Received: 7 December 2022 / Accepted: 9 February 2023

Abstract

A high-performance gas sensor operating at room temperature is always favourable since it simplifies the device fabrication and lowers the operating power by eliminating a heater. Herein, we fabricated the ammonia (NH_3) gas sensor by using Au nanoparticle-decorated TiO_2 nanosheets, which were synthesized via two distinct processes: (1) preparation of monolayer TiO_2 nanosheets through flux growth and a subsequent chemical exfoliation and (2) decoration of Au nanoparticles on the TiO_2 nanosheets via hydrothermal method. Based on the morphological, compositional, crystallographic, and surface characteristics of this low-dimensional nano-heterostructured material, its temperature- and concentration-dependent NH_3 gas-sensing properties were investigated. A high response of ~ 2.8 was obtained at room temperature under 20 ppm NH_3 gas concentration by decorating Au nanoparticles onto the surface of TiO_2 nanosheets, which generated oxygen defects and induced spillover effect as well.

Keywords TiO_2 nanosheet · Au nanoparticle · Ammonia · Gas sensor · Room temperature

Introduction

Serious safety issues like toxic gas leakage, explosion, and fire events frequently burst out due to storage or piping defects in industrial sites dealing with various oxidizing, reducing, and high-pressure hazardous chemical gases [1–9]. Various sensors such as electric capacity-, surface acoustic wave-, catalytic combustion-, optical-, electrochemical-, and semiconductor-type with different operating mechanisms have been developed to prevent these risks in advance [10–15].

Jeong Yun Hwang and Yerin Lee had equal contribution as co-first authors.

Supplementary Information The online version contains supplementary material available at https://doi.org/10.1186/s11671-023-03798-5.

✉ Myung Sik Choi, ms.choi@knu.ac.kr; ✉ Changhyun Jin, z8015026@yonsei.ac.kr; ✉ Kyu Hyoung Lee, khlee2018@yonsei.ac.kr | [1]Department of Materials Science and Engineering, Yonsei University, Seoul 03722, South Korea. [2]KIURI Institute, Yonsei University, Seoul 03722, South Korea. [3]Department of Materials Science and Engineering, University of Seoul, Seoul 02504, South Korea. [4]Department of Materials Science and Engineering, Dankook University, Cheonan 31116, South Korea. [5]Chemland Co., Ltd., Gunpo 15850, South Korea. [6]Faculty of Nanotechnology and Advanced Materials Engineering, Sejong University, Seoul 05006, South Korea. [7]School of Nano, Materials Science and Engineering, Kyungpook National University, Sangju 37224, South Korea.

Although semiconductor-type sensors have lower selectivity and reliability than electrochemical sensors [16, 17], their simple operation, economically feasible manufacturing process, possible miniaturization, and device compatibility have drawn much attention [18, 19]. The semiconductor-type sensors utilize metal oxides (SnO_2, ZnO, In_2O_3, WO_3, Ga_2O_3, TiO_2, CuO, TeO_2, NiO, etc.) as sensing materials [20–22]. Among many metal oxides, TiO_2 is one of the promising candidates for sensing materials since it has various crystal phases (anatase, rutile, and brookite) [23, 24] and generates carriers [25, 26]. Moreover, multiple forms of TiO_2 with controlled defect structures can be easily prepared via the sulfuric acid method, chlorine method, chemical vapour deposition (CVD) method, sol–gel method, and anodization method [27, 28]. The easily manipulated defect structures of TiO_2 are ideal for sensing gas molecules of interest. Different surface atomic sites [29, 30], defects [31], and cross-sectional areas of nanosheets [32] can selectively sense gas molecules with different electron affinities.

Recently, sensitive and selective sensing of ammonia (NH_3) gas, which is highly corrosive, toxic, yet colourless, has become indispensable along with the increasing use of NH_3 gas as a non-polluting fuel like hydrogen [33, 34]. Benefitting from easily engineered dimensions and defect structures of TiO_2, 0- and 1-dimensional TiO_2-based nanostructures and additional nano-heterostructures were found to be effective in sensing NH_3 gas with high selectivity, sensitivity, and stability at room temperature [35–40]. Herein, we fabricated the 2-dimensional TiO_2-based nano-heterostructures to improve NH_3 gas-sensing performance at room temperature. TiO_2 nanosheets (NSs) were first synthesized through flux growth and subsequent chemical exfoliation. This is because the flux growth method is advantageous for simultaneously obtaining large single crystals and large monolayer structures [41, 42]. Au nanoparticles (NPs) were then decorated onto the surface of the TiO_2 NSs by hydrothermal method. The high response of ~ 2.8, twice as high as that of the pristine TiO_2 NSs, was obtained at an NH_3 gas concentration of 20 ppm due to the oxygen defects generated in the TiO_2 NSs as well as the spillover effect activated in the presence of Au NPs [43, 44].

Experimental procedure

As illustrated in Fig. 1a, $K0.8Ti_{1.73}Li_{0.27}O_4$ (KTLO) was first synthesized via a flux method to fabricate TiO_2 NSs. Powders of TiO_2 (99.9%, Grand C&M), K_2CO_3 (99.5%, Samchun Chemicals), and Li_2CO_3 (99.0%, Junsei) were used as starting materials, and MoO_2 (99.5%, Samchun Chemicals) was added as a flux. Each powder was weighed in stoichiometry and mixed in a mortar. The mixed powder was put into a platinum (Pt) crucible and calcinated at 1200 °C for 10 h in air. After the calcination, it was slowly cooled to 900 °C for 50 h, followed by natural cooling. KTLO powder was obtained once the mixed powder was washed with distilled water at 80 °C to remove K_2MoO_4. The KTLO powder was converted to $H_{1.07}Ti_{1.73}O_4{\cdot}H_2O$ (HTO) via an acid treatment process performed for 5 days using 0.5 M hydrochloric acid (HCl, Daejung). The HTO powder (1.2 g) was stirred in a mixed solution of tetrabutylammonium hydroxide (TBAOH, 10.26 cc) and distilled (DI) water (300 cc) with a magnetic bar for 14 days to exfoliate TiO_2 NS. Finally, the TiO_2 NSs were obtained after centrifuging (6000 rpm, 10 min) and subsequent filtering (membrane in DI water, 3 days) of the TiO_2 NS-containing mixed solutions.

Au NPs were simply decorated onto the surface of TiO_2 NSs via the hydrothermal method, as shown in Fig. 1b. The precursor of Au was prepared by stirring $HAuCl_6{\cdot}H_2O$ (0.23 g) and 2-propanol (10 g) for 12 h. The mixture of the Au precursor ($HAuCl_6{\cdot}H_2O$, 1 ml), colloid of TiO_2 NSs (4 ml), and distilled water (40 ml) was reacted in an autoclave at 70 °C for 4 h. The Au NP-decorated TiO_2 NSs were obtained once the product of the hydrothermal reaction was washed in a mixed solution of DI water and ethanol using a centrifuge.

To characterize the morphology, crystallinity, composition, chemical bonding, and surface defect of the pristine and Au NP-decorated TiO_2 NSs, several analyses using field emission scanning electron microscopy (FE-SEM, JEOL-7001F, Jeol Ltd.), field emission transmission electron microscopy (FE-TEM, Talos F2000X, Thermo Fisher Scientific) with high-angle annular dark field (HAADF), atomic force microscopy (AFM, Park systems), powder X-ray diffraction (PXRD, Smartlab, Rigaku), energy-dispersive X-ray spectroscopy (EDX), X-ray photoelectron spectroscopy (XPS, K-Alpha, Thermo Fisher Scientific), Raman spectroscopy (LabRam Aramis, Horriba Jovin-Yvon), and photoluminescence (PL, LabRam Aramis, Horriba Jovin-Yvon) were carried out.

Sensing properties of the pristine and Au NP-decorated TiO_2 NSs for various gases (NH_3, H_2S, CH_3COCH_3, C_6H_6, C_2H_5OH, NO_2) were measured using the specially designed gas-sensing measurement system (Supporting Information (SI), Fig. S1), in which sensing materials were deposited on an alumina substrate masked with Au electrode by the drop-off technique. Gas sensing was performed for temperatures ranging from 30 to 110 °C with different gas concentrations (1, 2, 6, 10, and 20 ppm). The response was measured as a change in resistance before (R_a) and after (R_g) target gas injection. Oxidizing

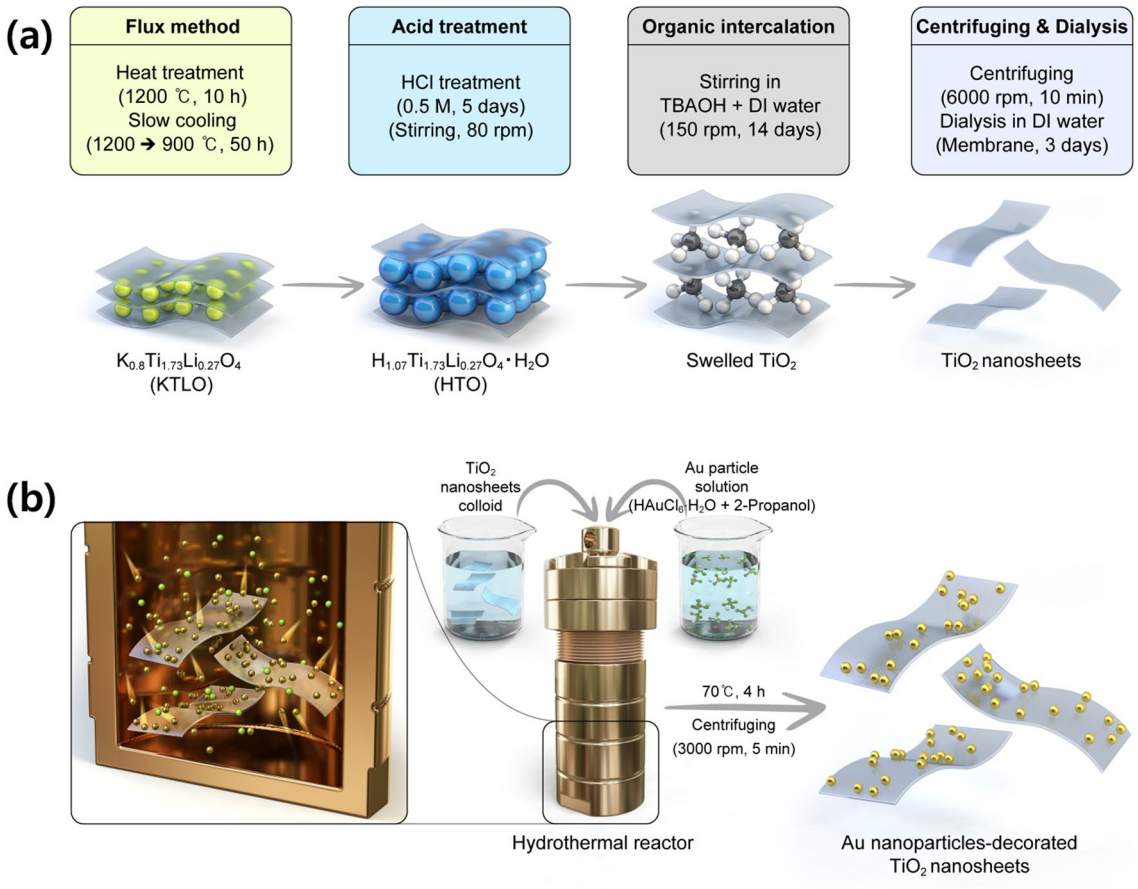

Fig. 1 Schematic diagrams for the process of synthesizing **a** TiO_2 nanosheets via combined process of flux method and exfoliation and **b** Au nanoparticle-decorated TiO_2 nanosheets via hydrothermal method

gas and reducing gas were expressed as $R = R_g/R_a$ and $R = R_a/R_g$, respectively. Response time and recovery time were calculated as the time to reach 90% of the final resistance in the presence and absence of the target gas, respectively.

Results and discussion

Figure 2a, b, and SI, Fig. S2a show the SEM and TEM images of the pristine TiO_2 NSs with uneven and serpentine-like morphology. The TiO_2 NS thickness of ~ 1.4 nm estimated from the AFM image (SI, Fig. S2b) indicates a successful insertion of TBA^+ ion between monolayer TiO_2 sheets just before the exfoliation (Fig. 1a), because the thickness of monolayer TiO_2 NS (~ 0.5 nm) and the size of adsorbed TBA^+ ion are approximately 0.5 and 0.9 nm, respectively [45]. Monodispersed Au NPs with an average diameter of 10–30 nm were decorated onto the surface of TiO_2 NSs via the simple and scalable hydrothermal process (Fig. 1b), as shown in Fig. 2c, d. The decorated Au NPs were not detached from TiO_2 NSs even after ultrasonication for 24 h.

Crystal structure, chemical bonding, and defect structure of the pristine and Au NP-decorated TiO_2 NSs were examined using XRD, Raman, PL, and XPS since the gas-sensing properties of semiconducting metal oxides are strongly correlated with these structural characteristics. Observed peaks in XRD analysis (Fig. 3a) are well matched to the planes of (0*l*0), which confirms the 2-dimensional sheet-like structure of TiO_2 NSs [46]. This 2-dimensional feature is maintained even after the hydrothermal process for Au NPs decoration. Peaks for Au are not detected, suggesting that the Au NPs with uniform nm-scale size are decorated as confirmed in the TEM image (Fig. 2d). The presence of such Au NPs can be clearly confirmed through high-resolution transmission electron microscopy (HRTEM) (SI, Fig. S3). However, the HRTEM image showed that the monolayer of TiO_2 was too thin (~ 0.5 nm); therefore, the interplanar spacing could not be clearly observed. Changes in bonding characteristics and defect structures of TiO_2 NSs after

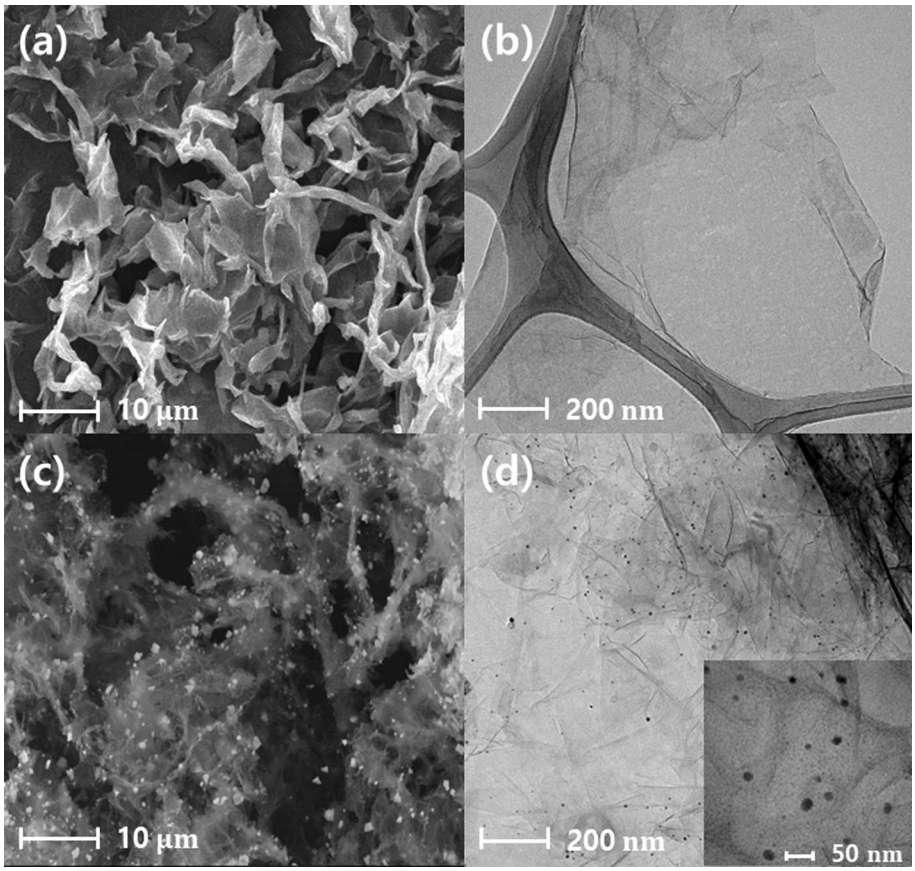

Fig. 2 **a** SEM and **b** TEM images showing the morphology of the pristine TiO_2 nanosheets. **c** SEM and **d** TEM images of the Au nanoparticle-decorated TiO_2 nanosheets. Inset in (**d**) shows the HADDF image

the decoration of Au NPs are also investigated. In Raman spectra (Fig. 3b), peaks corresponding to the TiO_2 NS (196, 283, 447, 706, and 784 cm^{-1}) are observed both in the pristine and Au NP-decorated TiO_2 NSs [47], suggesting no significant changes in Ti–O bonding states due to the Au NP decoration. This is also confirmed by XPS analysis, as represented in Fig. 3c, 3d. Peaks for Ti 2 s, Ti 2p, Ti 3 s, Ti 3p, and O 1 s [48] observed in the pristine TiO_2 NSs are also detected in the Au NP-decorated TiO_2 NSs at almost the same binding energies (peaks for Ti $2p_{3/2}$ and Ti $2p_{1/2}$ at 458.9 and 464.7 eV, respectively in Fig. 3d). The negligible change in the Ti–O bonding after the Au NP decoration can be attributed to the low reaction temperature (70 °C) of the hydrothermal process. On the other hand, the peak of Au 4f is clearly observed in XPS spectra of the Au NP-decorated TiO_2 NSs (Fig. 3c). Different binding energies for Au (83.8 and 87.5 eV) and Au^{3+} (85.2 and 88.9 eV) are confirmed by the peak analysis (Fig. 3e), indicating the presence of metal Au NPs and the bonding between the Au NPs and TiO_2. However, defect structures are changed by the Au NP decoration. According to the PL spectra (SI, Fig. S4), the peak intensities of the Au NP-decorated TiO_2 NSs corresponding to defect structures of oxygen vacancies and Ti interstitials (425 nm and 525 nm) [49, 50] are considerably lower than those measured in the pristine TiO_2 NSs. The surface oxygen defects, which play a critical role in gas sensing, are generated after the Au NP decoration. As shown in Fig. 3f, O 1s spectra are deconvoluted into three binding states: Ti–O lattice oxygen (O_a at ~ 530.3 eV), vacant oxygen (O_b at ~ 531.8 eV), and chemisorbed oxygen (O_c at ~ 532.8 eV). It is noted that the density of O_b was increased from 7.9 to 9.1% after decorating Au NPs. Unlike the Ti–O lattice oxygen binding state, the other two binding states played an important role in accelerating the properties of n-type semiconductors. When the vacancies of oxygen (O_b in Fig. 3f) increased, the ratio of fixed charge Ti ions increased. Therefore, the electrons acting as the main carriers of mobile charges also increased. Moreover, with regard to TiO_2, the electrons acting as the main carriers of mobile charges also increased because the increase in chemisorbed oxygen (Au_2O_3 in Fig. 3e and O_c in Fig. 3f) provided the same effect as that provided by disappearing O. In general, a heterointerface occurring in a pristine metal oxide nanostructure is commonly accompanied by a carrier transfer [51]. However, in our

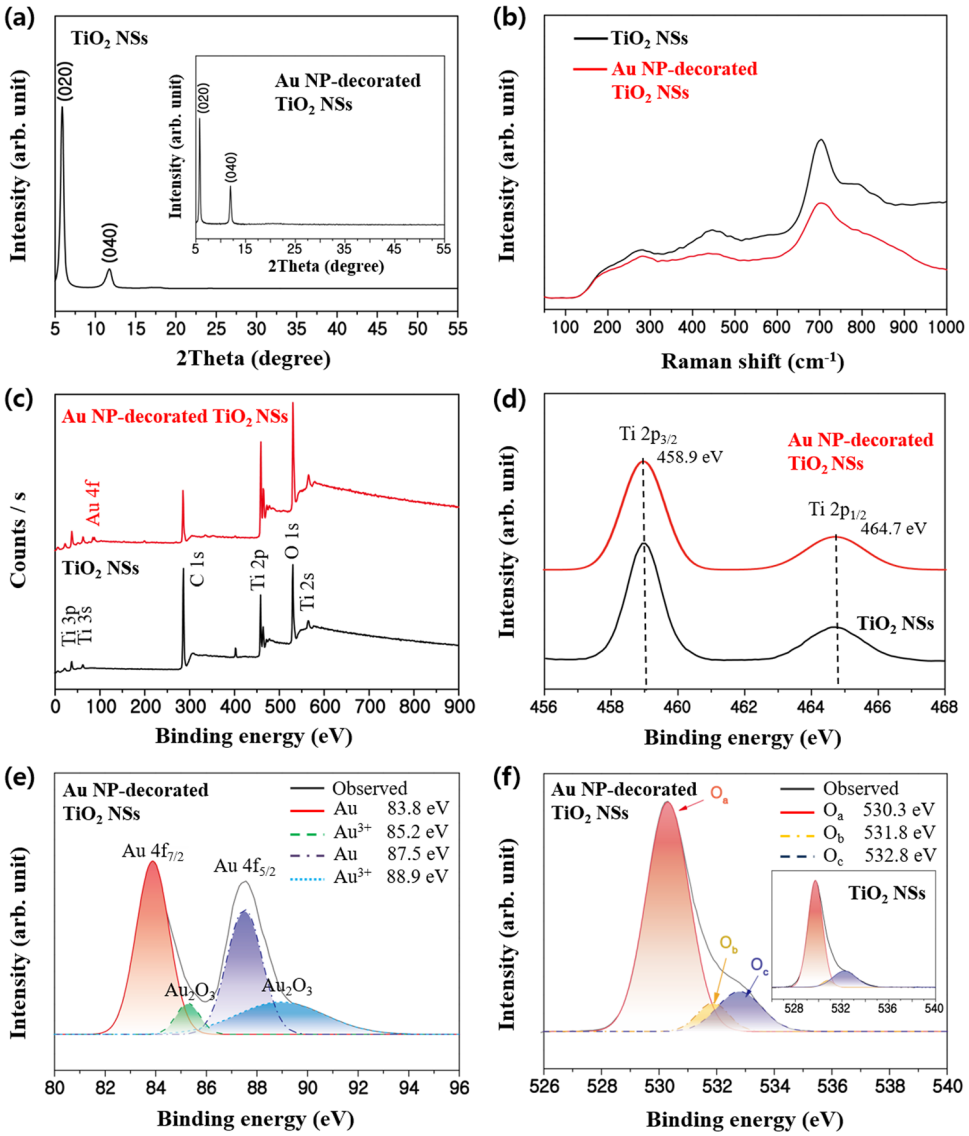

Fig. 3 **a** XRD patterns, **b** Raman spectra, and **c**–**f** XPS surveys of the pristine and Au nanoparticle-decorated TiO_2 nanosheets

study, when Au was decorated onto TiO_2 NSs, the overall Ti frame was maintained according to the Raman (Fig. 3b) and XPS (Fig. 3d) spectra. Meanwhile, O was considered to be locally chemisorbed with Au (Au_2O_3 in Fig. 3e and O_c in Fig. 3f) or to have acted as a vacancy defect (O_b in Fig. 3f).

To investigate the reactivity of the pristine and Au NP-decorated TiO_2 NSs with NH_3 gas correlated to the overall characteristics of morphology, chemical bonding, and surface defects characterized as above, their responses under NH_3 gas concentrations of 1–20 ppm at room temperature were measured (Fig. 4a, b). Owing to the n-type semiconducting nature of TiO_2, its resistance decreased when TiO_2 chemically reacted with the reducing NH_3 gas. In the initial state, the reducing NH_3 gas supplied electrons to the TiO_2 semiconductor. The response of the Au NP-decorated TiO_2 NSs is significantly improved in reference to that of the pristine TiO_2 NSs, even at a low concentration of 1 ppm. Moreover, considering the high sensing process temperatures (200–300 °C) of most semiconducting metal oxides [52, 53], sensitive sensing demonstrated at room temperature suggests that this low-dimensional nano-heterostructured material is a promising candidate for NH_3 gas-sensing materials. Dynamic responses for varying NH_3 gas concentrations are shown in Table S1. In both samples, the response gradually decreased when the concentration of NH_3 gas increased. The high response of ~ 2.8 is achieved with Au NP-decorated TiO_2 NSs at 20 ppm NH_3 gas concentration, which is approximately 6 times higher than that obtained with the pristine TiO_2 NSs (Fig. 4c). The ionization of oxygen

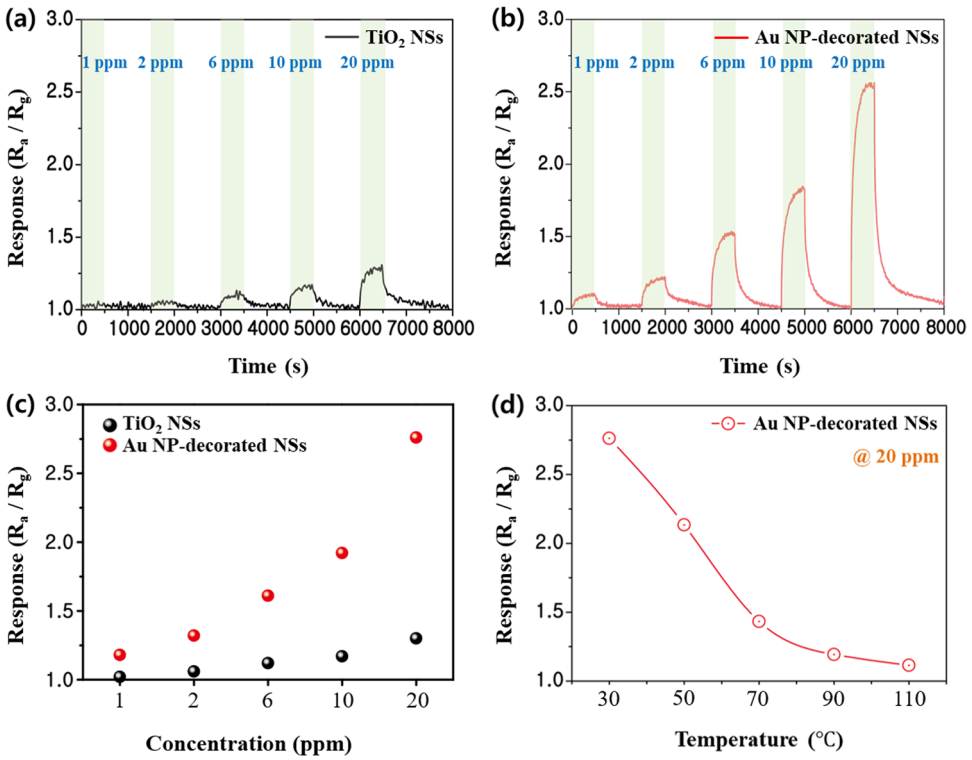

Fig. 4 NH_3 gas concentration-dependent responses at room temperature of **a** the pristine TiO_2 nanosheets and **b** Au nanoparticle-decorated TiO_2 nanosheets. **c** Comparison of the NH_3 gas concentration-dependent responses at room temperature between the pristine and Au nanoparticle-decorated TiO_2 nanosheets. **d** Response of the Au nanoparticle-decorated TiO_2 nanosheets according to the process temperature under 20 ppm NH_3 gas concentration

and the adsorption of NH_3 gas molecules activated by the spillover effect from the decorated Au NPs are the physics behind the improved response [54]. Conventionally, the response of a semiconductor increases with temperature as more carriers are generated at high temperatures. In contrast, the opposite trend is observed in the response of the Au NP-decorated TiO_2 NSs shown in Fig. 4d. This phenomenon can be attributed to the thin 2D structure of the sample used herein. When the temperature increased, the sample exhibited the properties of a metal rather than those of a semiconductor. Therefore, the number of carriers involved in sensing decreased with temperature. Room-temperature sensing can be understood with the following ionization processes, which occurs below 100 °C [55].

$$O_{2(gas)} \leftrightarrow O_{2(ads)} \tag{1}$$

$$O_{2(ads)} + e^{-} \rightarrow O^{-}_{2(ads)} \tag{2}$$

Additionally, Au NP-decorated TiO_2 NSs can selectively sense NH_3 gas at room temperature. The responses to other gases such as H_2S, CH_3COCH_3, C_6H_6, C_2H_5OH, and NO_2 were 1.41, 1.59, 2.26, 2.06, and 1.43, respectively (SI, Fig. S5). Hence, the selectivity of Au-NP-decorated TiO_2 NSs in sensing NH_3 can be considered to be the best. Long-term stability of Au NP-decorated TiO_2 NSs was confirmed by measurement of sensing dynamics after 1 month, which shows almost same behaviour as shown in SI, Fig. S6. However, humidity performance revealed a slight decrease in response (SI, Fig. S7). Herein, the samples with and without the effect of humidity showed similar responses in the three experiments repeated under the same conditions. Hence, a comparative analysis, as presented in Table 1, was conducted to demonstrate the improved performance of the proposed sensor. [5, 37, 56–61].

The NH_3 gas-sensing mechanism for the Au NP-decorated TiO_2 NSs is closely related to functions of the hetero-structures between metal and metal oxide: (1) electronic sensitization with oxygen or adsorbed catalytic metal and

Table 1 Comparison between the NH_3 gas-sensing properties of TiO_2-based gas sensors with the present optimized gas sensor

Sensor	NH_3 conc (ppm)	Response (R_a/R_g)	Temp. (°C)	Refs
TiO_2 nanotube	1000	~2.1	100	[56]
Tanninsulfinic acid-doped polyaniline-TiO_2 composite	20	1.5	RT	[57]
Cellulose/TiO_2/PANI composite nanofibers	250	~6.5	RT	[58]
TiO_2 nanowire	50	0.12	RT	[37]
GO/TiO_2 composite	100	0.383	RT	[5]
PANi-TiO_2 film	23	1.7	RT	[59]
TiO_2/PPy	30	3.52	RT	[60]
TiO_2/SnO_2 thick film	200	~2	250	[61]
Au nanoparticles decorated TiO_2 nanosheet	20	2.68	RT	Present work

(2) chemical sensitization between target gas and catalytic metal or semiconductor surface [62]. For example, the electron affinity of the oxygen adsorbed on the Au-Np-decorated TiO_2 NS surface is 1.46 eV [63] and that of the TiO with an oxygen vacancy is 1.19 eV [64]. Hence, oxygen removes electrons from the TiO_2 surface and ionizes the surface as shown in Eq. (2). An electron depletion layer (EDL) is consequently formed under the TiO_2 surface. Given that Au efficiently decomposes the oxygen (from O_2 to O_2^-) and ammonia (from NH_3 to N_2 or NO) adsorbed onto the TiO_2 surface and helps to form highly reactive ionic species, electron transfer occurs actively. In addition, because Au and TiO_2 have work functions of 4.86–4.92 eV [65] and 4.34 eV [66], respectively, a Schottky junction [67], in which electrons move only from the TiO_2 side to the Au side, occurs locally. Therefore, this interface also increases the thickness of the EDL in the air state. However, when NH_3 gas is injected in this state, the following reaction occurs [68, 69].

$$4NH_{2(ads)} + 3O^-_{2(ads)} \rightarrow 2N_2 + 6H_2O + 3e^- \quad (3)$$

$$4NH_{2(ads)} + 5O^-_{2(ads)} \rightarrow 4NO + 6H_2O + 5e^- \quad (4)$$

Additional electrons are supplied to the surface of TiO_2 and the thickness of the EDL formed inside the surface is reduced, resulting in a further decrease in resistance. However, when the NH_3 gas is desorbed, the original EDL thickness is restored owing to the influence of air on the TiO_2 surface. In summary, the primary gas-sensing mechanism was understood in terms of the conductive channelling width of the semiconductor related to the thickness of the carrier depletion layer [37], where potential difference [70, 71] and energy band diagram [72, 73] models at heterogeneous interfaces (Au NPs and TiO_2 NSs) could be used.

Conclusions

Au nanoparticle-decorated TiO_2 nanosheets are prepared via combination of flux growth-exfoliation and hydrothermal method, and their NH_3 gas-sensing properties were measured at process temperatures of 30–110 °C under different NH_3 gas concentrations (1–20 ppm). NH_3 gas was selectively detected by using the pristine monolayer TiO_2 nanosheets even at room temperature. The Au nanoparticle decoration triggered the generation of oxygen defects, which activated the reaction with NH_3 gas molecules, and also induced the spillover effect. Due to this synergetic effect, response of Au nanoparticle-decorated TiO_2 nanosheets can be significantly improved and reaches ~2.8 at room temperature under 20 ppm NH_3 gas concentration. Proposed design concept of low-dimensional nano-heterostructured sensing material and kinetics of gas sensing at room temperature are expected to be utilized to develop and optimize properties and performances of semiconducting metal oxide-based gas sensors.

Acknowledgements Not applicable.

Author contributions KHL, CJ, and MSC conceived the study, and designed the experiments. JYH, YL, and GHL synthesized the samples and measured the gas-sensing properties. SYL performed and analysed the XRD. HSK and HJP carried out the PL and XPS analysis. SIK, SJK, and BZL analysed the microstructures. JYH, CJ, and KHL co-wrote the manuscript. All the authors discussed the results and commented on the manuscript.

Funding This research was supported by the Basic Science Research Program through the National Research Foundation of Korea (NRF) funded by the Ministry of Science and ICT (2022R1A2C2005210), the Ministry of Education (2019R1A6A1A11055660), and the Ministry of Science and ICT (MSIT) (NRF-2021R1A5A8033165). This work was supported by the Industrial technology innovation project (20011034, Development of titania nano materials technology for high performance suncare for broadband UV protection) funded by the Ministry of Trade, Industry & Energy (MOTIE, Korea). This study was also supported by Samsung Electronics Co., Ltd. (IO201216–08204-01). Seung Yong Lee and Changhyun Jin were supported by the Korea Initiative for fostering University of Research and Innovation (KIURI) Program of the National Research Foundation (NRF) funded by the Korean government (MSIT) (NRF-2020M3H1A1077207).

Availability of data and material All the data are available from the corresponding author on reasonable request.

Declarations

Ethics approval and consent to participate Not applicable.

Consent for publication Not applicable.

Competing interests The authors declare no competing interests.

References

1. Wang Z, Sackmann A, Gao S, Weimar U, Lu G, Liu S, Zhang T, Barsan N. Study on highly selective sensing behavior of ppb-level oxidizing gas sensors based on Zn_2SnO_4 nanoparticles immobilized on reduced graphene oxide under humidity conditions. Sens Actuators B-Chem. 2019;285:590–600.
2. Sun G-J, Lee JK, Choi S, Lee WI, Kim HW, Lee C. Selective oxidizing gas sensing and dominant sensing mechanism of n-CaO-decorated n-ZnO nanorod sensors. ACS Appl Mater Interfaces. 2017;9:9975–85.
3. Simonetti EAN, Oliveira TC, Machado ÁEC, Silva AAC, Santos AS, Cividanes LS. TiO_2 as a gas sensor: the novel carbon structures and noble metals as new elements for enhancing sensitivity—a review. Ceram Int. 2021;47:17844–76.
4. Ramanavicius S, Tereshchenko A, Karpicz R, Ratautaite V, Bubniene U, Maneikis A, Jagminas A, Ramanavicius A. TiO_{2-x}/TiO_2-structure based 'Self-Heated' sensor for the determination of some reducing gases. Sensors. 2020;20:74.
5. Lee E, Lee D, Yoon J, Yin Y, Lee YN, Uprety S, Yoon YS, Kim D-J. Enhanced gas-sensing performance of GO/TiO_2 composite by photocatalysis. Sensors. 2018;18:3334.
6. Ramanavicius S, Ramanavicius A. Insights in the application of stoichiometric and non-stoichiometric titanium oxides for the design of sensors for the determination of gases and VOCs (TiO_{2-x} and Ti_nO_{2n-1} vs. TiO_2). Sensors. 2020;20:6833.
7. Sowmya B, John A, Panda PK. A review on metal-oxide based p-n and n-n heterostructured nano-materials for gas sensing applications. Sens Int. 2021;2:100085.
8. Srivastava S. Study of gas sensor detection for NO_x gas: a review. Mater Today Proc. 2021;37:3709–12.
9. Gomes JBA, Rodrigues JJPC, Rabêlo RAL, Kumar N, Kozlov S. IoT-enabled gas sensors: technologies, applications, and opportunities. J Sens Actuator Netw. 2019;8:57.
10. Mohankumar P, Ajayan J, Yasodharan R, Devendran P, Sambasivam R. A review of micromachined sensors for automotive applications. Measurement. 2019;140:305–22.
11. Hallil H, Dejous C, Hage-Ali S, Elmazria O, Rossignol J, Stuerga D, Talbi A, Mazzamurro A, Joubert P-Y, Lefeuvre E. Passive resonant sensors: trends and future prospects. IEEE Sens J. 2021;21:12618–32.
12. Khan MAH, Rao MV, Li Q. Recent advances in electrochemical sensors for detecting toxic gases: NO_2, SO_2 and H_2S. Sensors. 2019;19:905.
13. Balasubramani V, Chandraleka S, Rao TS, Sasikumar R, Kuppusamy MR, Sridhar TM. Review–recent advances in electrochemical impedance spectroscopy based toxic gas sensors using semiconducting metal oxides. J Electrochem Soc. 2020;167:037572.
14. Liu H, Zhang L, Li KHH, Tan OK. Microhotplates for metal oxide semiconductor gas sensor applications-towards the CMOS-MEMS monolithic approach. Micromachines. 2018;9:557.
15. Wang Y, Liu D, Yin J, Shang Y, Du J, Kang Z, Wang R, Chen Y, Sun D, Jiang J. An ultrafast responsive NO_2 gas sensor based on a hydrogen-bonded organic framework material. Chem Commun. 2020;56:703–6.

16. Cui F, Zhou Z, Zhou HS. Molecularly imprinted polymers and surface imprinted polymers based electrochemical biosensor for infectious diseases. Sensors. 2020;20:996.
17. Jin H, Guo H, Gao X, Gui R. Selective and sensitive electrochemical sensing of gastrodin based on nickel foam modified with reduced graphene oxide/silver nanoparticles complex-encapsulated molecularly imprinted polymers. Sens Actuators B-Chem. 2018;277:14–21.
18. Korotcenkov G. Current trends in nanomaterials for metal oxide-based conductometric gas sensors: advantages and limitations. Part 1: 1D and 2D nanostructures. Nanomaterials. 2020;10:1392.
19. Nikolic MV, Milovanovic V, Vasiljevic ZZ, Stamenkovic Z. Semiconductor gas sensors: materials, technology, design, and application. Sensors. 2020;20:6694.
20. Dey A. Semiconductor metal oxide gas sensors: a review. Mater Sci Eng B. 2018;229:206–17.
21. Lin T, Lv X, Hu Z, Xu A, Feng C. Semiconductor metal oxides as chemoresistive sensors for detecting volatile organic compounds. Sensors. 2019;19:233.
22. Mahajan S, Jagtap S. Metal-oxide semiconductors for carbon monoxide (CO) gas sensing: a review. Appl Mater Today. 2020;18:100483.
23. Yi Z, Zeng Y, Wu H, Chen X, Fan Y, Yang H, Tang Y, Yi Y, Wang J, Wu P. Synthesis, surface properties, crystal structure and dye-sensitized solar cell performance of TiO_2 nanotube arrays anodized under different parameters. Results Phys. 2019;15:102609.
24. Kang M, Kim SW, Park HY. Optical properties of TiO_2 thin films with crystal structure. J Phys Chem Solids. 2018;123:266–70.
25. Meng A, Zhang L, Cheng B, Yu J. Dual cocatalysts in TiO_2 photocatalysis. Adv Mater. 2019;31:1807660.
26. Guo Q, Zhou C, Ma Z, Yang X. Fundamentals of TiO_2 photocatalysis: concepts, mechanisms, and challenges. Adv Mater. 2019;31:1901997.
27. Gonçalves RA, Toledo RP, Joshi N, Berengue OM. Green synthesis and applications of ZnO and TiO_2 nanostructures. Molecules. 2021;26:2236.
28. Noman MT, Ashraf MA, Ali A. Synthesis and applications of nano-TiO_2: a review. Environ Sci Pollut Res. 2019;26:3262–91.
29. Han Z, Qi Y, Yang Z, Han H, Jiang Y, Du W, Zhang X, Zhang J, Dai Z, Fletcher C, Wang Z, Liu J, Wu L, Lud G, Wang F. Recent advances and perspectives on constructing metal oxide semiconductor gas sensing materials for efficient formaldehyde detection. J Mater Chem C. 2020;8:13169–88.
30. Yuvaraja S, Bhyranalyar VN, Bhat SA, Surya SG, Yelamaggad CV, Salama KN. A highly selective electron affinity facilitated H_2S sensor: the marriage of tris(keto-hydrazone) and an organic field-effect transistor. Mater Horiz. 2021;8:525537.
31. Cao Y, Maitarad P, Gao M, Taketsugu T, Li H, Yan T, Shi L, Zhang D. Defect-induced efficient dry reforming of methane over two-dimensional Ni/h-boron nitride nanosheet catalysts. Appl Catal B: Environ. 2018;238:51–60.
32. Jo YK, Lee JM, Son S, Hwang S-J. 2D inorganic nanosheet-based hybrid photocatalysts: design, applications, and perspectives. J Photochem Photobiol C Photochem Rev. 2019;40:150–90.
33. Hu T-T, Liu F, Dou S, Zhong L-B, Cheng X, Shao Z-D, Zheng Y-M. Selective adsorption of trace gaseous ammonia from air by a sulfonic acid-modified silica xerogel: preparation, characterization and performance. Chem Eng J. 2022;443:136357.
34. Kwak D, Lei Y, Maric R. Ammonia gas sensors: a comprehensive review. Talanta. 2019;204:713–30.
35. Wu H, Huang H, Zhou J, Hong D, Ikram M, Rehman AU, Li L, Shi K. One-step synthesis of ordered Pd@TiO_2 nanofibers array film as outstanding NH3 gas sensor at room temperature. Sci Rep. 2017;7:14688.
36. Liu H, Shen W, Chen X. A room temperature operated ammonia gas sensor based on Ag-decorated TiO_2 quantum dot clusters. RSC Adv. 2019;9:24519.
37. Shooshtari M, Salehi A. Ammonia room-temperature gas sensor using different TiO_2 nanostructures. J Mater Sci Mater Electron. 2021;32:17371–81.
38. Zhou Y, Wang Y, Wang Y, Yu H, Zhang R, Li J, Zang Z, Li X. MXene $Ti_3C_2T_x$-derived nitrogen-functionalized heterophase TiO_2 homojunctions for room-temperature trace ammonia gas sensing. ACS Appl Mater Interfaces. 2021;13:56485–97.
39. Wang Y, Zhou Y, Wang Y, Zhang R, Li J, Li X, Zang Z. Conductometric room temperature ammonia sensors based on titanium dioxide nanoparticles decorated thin black phosphorus nanosheets. Sens Actuators B-Chem. 2021;349:130770.
40. Zhou Y, Li X, Wang Y, Tai H, Guo Y. UV illumination-enhanced molecular ammonia detection based on a ternary-reduced graphene oxide–titanium dioxide–Au composite film at room temperature. Anal Chem. 2019;91:3311–8.
41. Kawamura F, Umeda H, Morishita M, Kawahara M, Yoshimura M, Mori Y, Sasaki T, Kitaoka Y. Growth of a two-inch GaN single crystal substrate using the Na flux method. Jpn J Appl Phys. 2006;45:L1136–8.
42. Kim J, Choi J-W. Synthesis of large monolayer titania nanosheets through flux method. J Asian Ceram Soc. 2021;9:916–25.
43. Zhang X, Liu Y, Liu H, Liang T, Zhang P, Da Z. $FeSe_2$/Hematite nn heterojunction with oxygen spillover for highly efficient NO_2 gas sensing. Sens Actuators B-Chem. 2021;345:130357.
44. Liu B, Li K, Luo Y, Gao L, Duan G. Sulfur spillover driven by charge transfer between AuPd alloys and SnO_2. Chem Eng J. 2021;420:12988.
45. Park HJ, Lee SE, Park JY. Optical property of atomically thin titanium-oxide nanosheet for ultraviolet filtration. Thin Solid Films. 2017;636:99–106.
46. Lee SE, Jung SY, Seo J, Joo JH, Lee J, Kim Y-M, Lee KH, Kim YI, Park HJ. Anomalous electronic and protonic conductivity of 2D titanium oxide and low-temperature power generation using its protonic conduction. Adv Mater Interfaces. 2021;8:2101156.
47. Wan J, Chen W, Jia C, Zheng L, Dong J, Zheng X, Wang Y, Yan W, Chen C, Peng Q, Wang D, Li Y. Defect effects on TiO_2 nanosheets: stabilizing single atomic site Au and promoting catalytic properties. Adv Mater. 2018;30:1705369.
48. Wang H-Y, Soldemo M, Degerman D, Lömker P, Schlueter C, Nilsson A, Amann P. Direct evidence of subsurface oxygen formation in oxide-derived Cu by x-ray photoelectron spectroscopy. Angew Chem Int Ed. 2022;61:e202111021.
49. Samsudin EM, Hamid SBA, Juan JC, Basirun WJ, Kandjani AE. Surface modification of mixed-phase hydrogenated TiO_2 and corresponding photocatalytic response. Appl Surf Sci. 2015;359:883–96.
50. Das TK, Ilaiyaraja P, Sudakar C. Template assisted nanoporous TiO_2 nanoparticles: the effect of oxygen vacancy defects on photovoltaic performance of DSSC and QDSSC. Sol Energy. 2018;159:920–9.
51. Xia Y, Xu L, He S, Zhou L, Wang M, Wang J, Komarneni S. UV-activated WS_2/SnO_2 2D/0D heterostructures for fast and reversible NO_2 gas sensing at room temperature. Sens Actuators B-Chem. 2022;364:131903.
52. Deng Z, Meng G, Fang X, Dong W, Shao J, Wang S, Tong B. A novel ammonia gas sensors based on p-type delafossite $AgAlO_2$. J Alloys Compd. 2019;777:52–8.

53. Yao G, Yu J, Wu H, Li Z, Zou W, Zhu H, Huang Z, Huang H, Tang Z. P-type Sb doping hierarchical WO_3 microspheres for superior close to room temperature ammonia sensor. Sens Actuators B-Chem. 2022;359:131365.
54. Choi MS, Kim MY, Mirzaei A, Kim H-S, Kim S-I, Baek S-H, Chun DW, Jin C, Lee KH. Selective, sensitive, and stable NO_2 gas sensor based on porous ZnO nanosheets. Appl Surf Sci. 2021;568:150910.
55. Phawa C, Prayoonpokarach S, Sinthiptharakoon K, Chakthranont P, Sangkhun W, Faungnawakij K, Butburee T. Effects of matching facet pairs of TiO_2 on photoelectrochemical water splitting behaviors. ChemCatChem. 2020;12:2116–24.
56. Galstyan V, Comini E, Faglia G, Sberveglieri G. TiO_2 nanotubes: recent advances in synthesis and gas sensing properties. Sensors. 2013;13:14813–38.
57. Bairi VG, Bourdo SE, Sacre N, Nair D, Berry BC, Biris AS, Viswanathan T. Ammonia gas sensing behavior of tanninsulfonic acid doped polyaniline-TiO_2 composite. Sensors. 2015;15:26415–29.
58. Pang Z, Yang Z, Chen Y, Zhang J, Wang Q, Huang F, Wei Q. A room temperature ammonia gas sensor based on cellulose/TiO_2/PANI composite nanofibers. Colloids Surf A Physicochem Eng Asp. 2016;494:248–55.
59. Tai H, Jiang Y, Xie G, Yu J, Chen X, Ying Z. Influence of polymerization temperature on NH3 response of PANI/TiO_2 thin film gas sensor. Sens Actuators B Chem. 2008;129:319–26.
60. Tai H, Jiang Y, Xie G, Yu J, Zhao M. Self-assembly of TiO_2/polypyrrole nanocomposite ultrathin films and application for an NH_3 gas sensor. Int J Environ Anal Chem. 2007;87:539–51.
61. Jung JY, Lee CS. Characteristics of the TiO_2/SnO_2 thick film semiconductor as sensor to determine fish freshness. J Ind Eng Chem. 2011;17:237–42.
62. Ding Y, Guo X, Du B, Hu X, Yang X, He Y, Zhou Y, Zang Z. Low-operating temperature ammonia sensor based on Cu_2O nanoparticles decorated with p-type MoS_2 nanosheets. J Mater Chem C. 2021;9:4838–46.
63. Kristiansson MK, Chartkunchand K, Eklund G, Hole OM, Anderson EK, Ruette N, Kamińska M, Punnakayathil N, Navarro-Navarrete JE, Sigurdsson S, Grumer J, Simonsson A, Björkhage M, Rosén S, Reinhed P, Blom M, Källberg A, Alexander JD, Cederquist H, Zettergren H, Schmidt HT, Hanstorp D. High-precision electron affinity of oxygen. Nat Commun. 2022;13:5906.
64. Qu Z, Kroes G. Theoretical study of the electronic structure and stability of titanium dioxide clusters (TiO_2)n with n = 1–9. J Phys Chem B. 2006;110:8998–9007.
65. Sachtler WMH, Dorgelo GJH, Holscher AA. The work function of gold. Surf Sci. 1966;5:221–9.
66. Kashiwaya S, Morasch J, Streibel V, Toupance T, Jaegermann W, Klein A. The work function of TiO_2. Surfaces. 2018;1:73–89.
67. Wei Y, Wang X, Yi G, Zhou L, Cao J, Sun G, Chen Z, Bala H, Zhang Z. Hydrothermal synthesis of Ag modified ZnO nanorods and their enhanced ethanol-sensing properties. Mater Sci Semicond Process. 2018;75:327–33.
68. Wu K, Debliquy M, Zhang C. Room temperature gas sensors based on Ce doped TiO_2 nanocrystals for highly sensitive NH_3 detection. Chem Eng J. 2022;444:136449.
69. Rahimi S, Abdi Y, Arzi E. Impact of TiO_2/Graphene-Oxide coated on quartz crystal resonator on the sensing performance of NH_3, N_2 and ethanol at room temperature. Phys B. 2021;623:413348.
70. Tian X, Cui X, Lai T, Ren J, Yang Z, Xiao M, Wang B, Xiao X, Wang Y. Gas sensors based on TiO_2 nanostructured materials for the detection of hazardous gases: a review. Nano Mater Sci. 2021;3:390–403.
71. Seekaew Y, Pon-On W, Wongchoosuk C. Ultrahigh selective room-temperature ammonia gas sensor based on Tin–Titanium dioxide/reduced graphene/carbon nanotube nanocomposites by the solvothermal method. ACS Omega. 2019;4:16916–24.
72. Zeng G, Cao H, Chen W, Lutz J. Difference in device temperature determination using p-n-junction forward voltage and gate threshold voltage. IEEE Trans Power Electron. 2019;34:2781–93.
73. Tanaka H, Mori N. Modeling of carrier scattering in MOS inversion layers with large density of interface states and simulation of electron Hall mobility in 4H-SiC MOSFETs. Jpn J Appl Phys. 2020;59:031006.